DC and Transmission Line Models for a High Electron Mobility Transistor

DI-HUI HUANG, STUDENT MEMBER, IEEE, AND HUNG C. LIN, LIFE FELLOW, IEEE

Abstract—**Two improved dc models are developed for the output current–voltage characteristics and small-signal parameters of a GaAs high electron mobility transistor (HEMT). A simple analytical nonlinear charge control model for two-dimensional electron gas is introduced and included in one of the dc models. The HEMT is modeled as a transmission line for the microwave frequency ac analysis, and the microwave performance of the HEMT is predicted by the parameters obtained from fitting dc characteristics. Both dc and ac model predictions show a good agreement with experimental results of a 0.3 μm GaAs HEMT.**

I. INTRODUCTION

RECENTLY, there has been considerable interest in the development of the high electron mobility transistor (HEMT). This device is very promising for both microwave and high-speed circuit application [1]–[3]. It has demonstrated excellent small-signal and noise characteristics. Potential applications include low-noise discrete FET's for telecommunications [4], high-speed analog MMIC's for data acquisition systems, and LSI digital integrated circuits for supercomputers.

In order to optimize the operation of the device, one must obtain an accurate understanding of its physical behavior and have an in-depth knowledge of the various physical phenomena occurring in the device. In this connection, accurate simulation methods are clearly needed. In addition, models are necessary for simulation prior to very expensive fabrication.

To provide the basis for the development of HEMT technology, a number of dc models have been reported in the literature. Various degrees of success in fitting dc data have been achieved, but only a few authors have made comparisons with microwave frequency data. Roblin *et al.* [5] recently reported an analytical microwave model for HEMT's which showed reasonable agreement with measured Y parameters from 2 to 18.4 GHz, but their ac model is based on constant mobility for the derivation, which lacks physical background. Yeager and Dutton [6] reported a large-signal model which they compared with actual measured microwave data at 4 GHz. They obtained a fit of the drain bias dependence of the HEMT Y parameters with a 30–50 percent error.

Manuscript received December 13, 1988; revised April 15, 1989. This work was supported in part by the Allied-Signal Aerospace Technology Center, Columbia, MD.

The authors are with the Department of Electrical Engineering, University of Maryland, College Park, MD 20740.

IEEE Log Number 8929182.

In this paper, we shall attempt to reproduce simultaneously the dc characteristics and microwave performance of the HEMT using a unique set of physical device parameters. In Section II, two different dc models for HEMT's will be presented: one is a simple analytical model with linear charge control, and the other, a nonlinear charge control model. In Section III, we will also present a new transmission line model for microwave frequency analysis which is suitable for both MESFET's and HEMT's. Finally, in Section IV, our new models are compared with experimental measurement data.

II. DESCRIPTION OF THE DC MODELS

The two dc models for the HEMT's will be presented in this section. One is a simple analytical model using a more accurate empirical formula for electron velocity versus electric field; the other is a nonlinear charge control model.

A. Two-Dimensional Electron Gas (2DEG) at Thermal Equilibrium

The gradual-channel approximation and Boltzmann transport theory are used as a basis for modeling the current characteristics of the two-dimensional electron gas. The first requires a relationship between the applied gate-to-channel potential and the electron gas concentration. Instead of working directly with one of these relations, however, we have found it more convenient to represent carrier concentration with piecewise empirical formulas. In 1982, Drummod *et al.* [7] suggested a linear charge control model as follows:

$$n_s = \frac{\epsilon_{\mathrm{AlGaAs}}}{q(d_i + d_d + \Delta d)}\left[V_g - V_{t0} - V(x)\right] \qquad (1)$$

where $\epsilon_{\mathrm{AlGaAs}}$ is the permittivity of AlGaAs; $d_i + d_d$ is the total thickness of the AlGaAs layer as shown in Fig. 1; V_{t0} is the threshold voltage; $\Delta d = \epsilon_{\mathrm{AlGaAs}} a/q \simeq 80$ (Å); and $a = 0.125 \times 10^{-12}$ (eV/cm^2).

This model is indeed adequate for analytical device modeling over certain ranges. However, for a large gate voltage, due to the neutralizing of donors in the AlGaAs layer, the 2DEG is saturated as shown in Fig. 2. There are few nonlinear models [8]–[10] for describing this nonlinear effect, but all these models require four or more fitting parameters which are inconvenient for device modeling. A two-section piecewise-nonlinear charge control model is

0018-9480/89/0900-1361$01.00

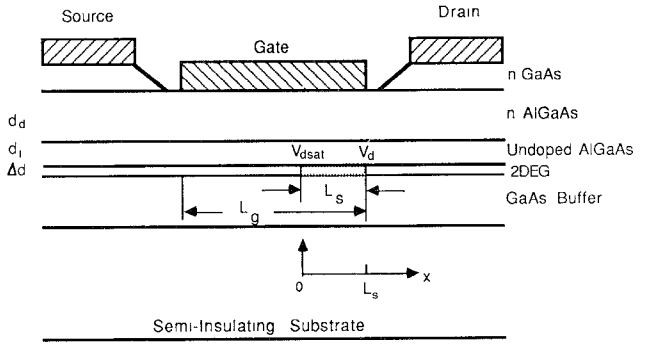

Fig. 1. High electron mobility transistor structure.

proposed as follows:

$$n_{s1}(V) = \frac{\epsilon_{\text{AlGaAs}}}{q(d_i + d_d + \Delta d)}\left[V_g - V_{t0} - V(x)\right], \quad V_g - V(x) \leq V_p \quad (2a)$$

$$n_{s2}(V) = \frac{A\left[V_g - V_{t0} - V(x)\right]}{1 + B\left[V_g - V_{t0} - V(x)\right]} + C, \quad V_g - V(x) > V_p. \quad (2b)$$

The first equation is the same as (1). A, B, and C are constants which can be determined analytically. There are two fitting parameters as shown in Fig. 2: 1) $p(<1)$, the point at which 2DEG concentration becomes nonlinear and 2) V_{ps}, the voltage at which 2DEG concentration equals the equilibrium concentration n_{s0}. V_p can be determined by (2a) as follows if $V(x) = 0$:

$$V_p = V_{t0} + \frac{q(d_i + d_d + \Delta d)\, pn_{s0}}{\epsilon_{\text{AlGaAs}}}. \quad (3)$$

The three constants A, B, and C are analytically determined by the following three boundary conditions: 1) $n_{s1}(V_p) = n_{s2}(V_p)$; 2) $\partial n_{s1}(V_p)/\partial V_g = \partial n_{s2}(V_p)/\partial V_g$; and 3) $n_{s2}(V_{ps}) = n_{s0}$. After manipulation, one obtains

$$A = \frac{\epsilon_{\text{AlGaAs}}}{q(d_i + d_d + \Delta d)}\left[\frac{\eta(V_1 - V_2)}{V_1(\eta - V_2) + V_2^2}\right]^2 \quad (4)$$

$$B = \frac{V_1 - V_2 - \eta}{V_1(\eta - V_2) + V_2^2} \quad (5)$$

$$C = n_{s0}\left[\frac{V_1(p\eta - V_2) + V_2^2}{V_1(\eta - V_2) + V_2^2}\right]^2 \quad (6)$$

where $V_1 = V_{ps} - V_{t0}$; $V_2 = V_p - V_{t0}$; and $\eta = n_{s0}(d_i + d_d + \Delta d)(1-p)/\epsilon_{\text{AlGaAs}}$. Fig. 2 illustrates that, with the optimum set of parameters, the $n_s(V)$ curve given by (2) is a very good approximation to the fully numerical self-consistent two-band models [8]. It appears that in order to accurately account for such important features as current pinch-off and saturation, as well as the position and magnitude of the transconductance peak, one needs to use a more accurate approximation for the $n_s(V)$ curve than is usually employed. It has also been demonstrated that the properly fitted functional form in (2) approximates the actual n_s curve very well.

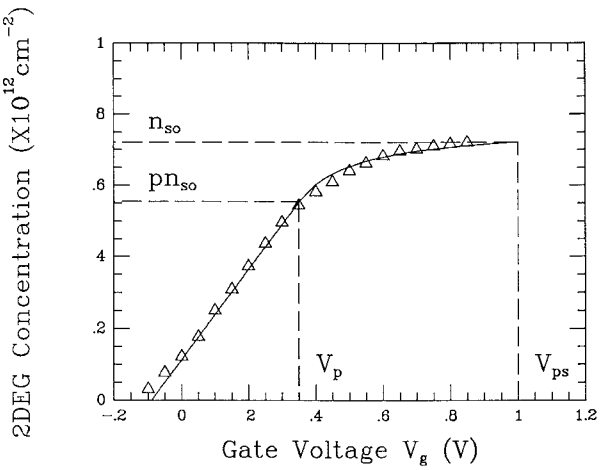

Fig 2. 2DEG concentration versus gate-to-channel voltage for GaAs/AlGaAs HEMT's Solid line: two-piece analytical model based on eq. (2). △: Fully numerical self-consistent two-band model [8].

B. Velocity-Field Model for 2DEG Electron

In this paper, we will first present the first-order simulation models for the HEMT's that are suitable for dc and small-signal ac simulations for both microwave and digital integrated circuits. Since many of the transport properties of the device are still under investigation, we have chosen to work within the drift-diffusion approximation of the Boltzmann transport equation, recognizing that the rigorous modeling of nonstationary and real-space transfer effects cannot be done at the circuit simulation level in an expedient manner. The use of the drift-diffusion approximation requires a stationary velocity–electric field curve. The commonly used empirical equation of electron velocity–field dependence, which was suggested by Trofimenkoff [11], is expressed as follows:

$$v(x) = \frac{\mu_l E(x)}{1 + \mu_l E(x)/v_s} \quad (7)$$

where $v(x)$ is the electron drift velocity, $E(x)$ the electric field, v_s the saturation drift velocity, and μ_l the low field mobility. However, the velocity–field dependence described by (7) can be improved to fit the experimental data better by using the empirical formula suggested by Giblin *et al.* [12]. The relationship they proposed is

$$v(x) = v_s\left[1 - \exp\left(-E(x)/E_s\right)\right] \quad (8)$$

where E_s is the saturation electric field. However, for certain semiconductors with two conduction band valleys, such as GaAs and InP, the velocity versus field curve has a peak, and hence a so-called negative resistance region, in which the drift velocity decreases with increasing field. In order to have the best simulation results, we use the following empirical formula, which is similar to Kroemer's model [13]:

$$v(x) = \frac{v_0 E(x)/E_0 + v_s\left[E(x)/E_0\right]^2}{1 + \left[E(x)/E_0\right]^2} \quad (9)$$

where $v_0 = \mu_l E_0$, E_0 being a fitting parameter (~ 3.0 kV/cm). In Fig. 3, we compare the velocity–field depen-

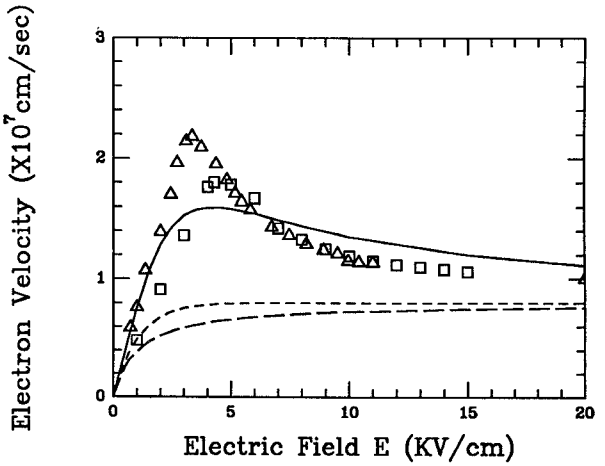

Fig. 3. Different approximations of velocity versus electric field curve. △: experimental data [14]; □: Monte Carlo simulation results [15]; solid line: eq. (9); dot line: eq. (8); dot–dash line: eq. (7). Here: $\mu_l = 7500$ cm^2/Vs, $v_s = 8\times10^6$ cm/s.

dence of (7), (8), and (9) to experimental data and simulation results. The solid line represent the v versus E curve of (9); the dashed and dot–dashed lines represent the curves of (7) and (8), respectively. The experimental data and simulation results are from [14] and [15]. As one can see from this figure, the empirical formula of (9) fits the experimental data much better than the formula of (7) and (8). Equation (9) will therefore be used to derive the analytical model of HEMT's with the linear charge control model, and (8) will be used to derive the dc nonlinear charge control model. It is found that the theoretical results are in excellent agreement with experimental data.

C. Analytical dc Linear Charge Control Model

In practical operation, the device is operated under the condition whereby the device has the maximum transconductance g_m. In this bias condition, the device is operating in the linear portion of Fig. 2. In this case, we can develop an analytical dc linear charge control model (eq. (1)) and a more accurate empirical formula of velocity versus field dependence (eq. (9)), as well as the current continuity equation:

$$I_{ds} = qn_s(x)v(x)W \tag{10}$$

where W is the gate width and q the electronic charge.

By solving (1), (9), and (10) simultaneously, one can have the following analytical I–V characteristics (a detailed derivation is given in Appendix):

$$I_{ds} = \beta\frac{(V_g - V_{t0})V_{ds} - V_{ds}^2/2}{1+\alpha V_{ds}} \tag{11}$$

where $\beta = \epsilon_{\mathrm{AlGaAs}}\mu_l W/(d_i + d_d + \Delta d)L_g$.

The above equation is similar to that proposed by Tiwari [16], but the coefficient α is different, as expressed in (12), which is dependent on the more accurate velocity versus field dependence relationship and on the source resistance R_s:

$$\alpha = \frac{v(x)/v_0}{E_0 L_g} + \beta R_s. \tag{12}$$

To obtain the saturation current and voltage, calculate $g_d = \partial I_d/\partial V_d$ and set $g_d = 0$ at saturation:

$$V_{d\,\mathrm{sat}} = \frac{\sqrt{1+2\alpha(V_g - V_{t0})} - 1}{\alpha}. \tag{13}$$

After channel current is saturated, Poisson's equation is solved as Park [17] suggested:

$$\frac{\partial^2 V}{\partial x^2} = \frac{1}{\epsilon_{\mathrm{AlGaAs}}}\frac{J}{v_s} \tag{14}$$

where the current density $J = I_{d\,\mathrm{sat}}/W\Delta d$, and v_s is the carrier drift velocity at the saturation point. By using the following two boundary conditions: 1) $V(0) = V_{d\,\mathrm{sat}}$; 2) $\partial V(0)/\partial x = E_{d\,\mathrm{sat}} \simeq V_{d\,\mathrm{sat}}/L_g$, as shown in Fig. 1, one can obtain an analytical expression for the reduced channel length L_s as follows:

$$L_s = \gamma\left[\sqrt{1+2(V_{ds} - V_{d\,\mathrm{sat}})/\gamma E_{\mathrm{sat}}} - 1\right] \tag{15}$$

where

$$\gamma = \frac{\epsilon_{\mathrm{AlGaAs}} v_s \Delta d W E_{\mathrm{sat}}}{I_{d\,\mathrm{sat}}}. \tag{16}$$

For the drain voltage greater than the saturation voltage, channel current is calculated by (11), but V_{ds} should be replaced by $V_{d\,\mathrm{sat}}$, and L_g, by $L_g - L_s$. Consequently, we obtain the current–voltage characteristics in both linear and saturation regions. In Section IV, we will compare the simulated results with the experimental data, which will show the excellent agreement of this analytical model.

D. Numerical dc Nonlinear Charge Control Model

In order to accurately determine the position and magnitude of the transconductance peak, our second model utilizes the nonlinear charge control (eq. (2)) and the velocity versus field dependence formula (eq. (8)).

Using $E(x) = -dV/dx$ and substituting (8) into (10) yields

$$\frac{dV}{\log\left[1 - I_{ds}/qv_s n_s(V)W\right]} = -E_s\,dx. \tag{17}$$

In the above equation, n_s should be replaced by either (2a) or (2b) depending on the different bias conditions.

For convenience of discussion, the following three quantities are defined:

$$V_a = V_g - V_{t0} - V_s \tag{18a}$$

$$V_b = V_p - V_{t0} \tag{18b}$$

$$V_c = V_g - V_{t0} - V_d. \tag{18c}$$

The above three voltage variables have clear physical meanings. V_a and V_c are the effective voltages at the source and drain ends of the channel, respectively, while V_b is the voltage at the boundary between the linear and nonlinear regions in Fig. 2. Because there are two different regions in Fig. 2, the following three source–drain bias conditions may occur:

Condition 1: Both the source and the drain terminal are biased in the nonlinear region in Fig. 2, i.e., $V_a > V_b$; $V_c > V_b$.

Condition 2: The source terminal is biased in the nonlinear region, while the drain is biased in the linear region in Fig. 2, i.e., $V_a > V_b$; $V_c \leqslant V_b$.

Condition 3: Both the source and the drain terminal are biased in the linear region in Fig. 2, i.e., $V_a \leqslant V_b$; $V_c \leqslant V_b$.

To predict the current–voltage characteristics of the HEMT, (2) has to be substituted into (17) depending the different bias conditions as follows.

Condition 1:

$$\int_{V_s}^{V_d} \frac{dV}{\log\left[1 - I_{ds}/qv_s n_{s2}(V)W\right]} = -\int_0^{L_g} E_s\, dx. \quad (19a)$$

Condition 2:

$$\int_{V_s}^{V_p} \frac{dV}{\log\left[1 - I_{ds}/qv_s n_{s2}(V)W\right]} + \int_{V_p}^{V_d} \frac{dV}{\log\left[1 - I_{ds}/qv_s n_{s1}(V)W\right]} = -\int_0^{L_g} E_s\, dx. \quad (19b)$$

Condition 3:

$$\int_{V_s}^{V_d} \frac{dV}{\log\left[1 - I_{ds}/qv_s n_{s1}(V)W\right]} = -\int_0^{L_g} E_s\, dx. \quad (19c)$$

Equation (19) describes the output I–V characteristics of HEMT's. Given V_{ds} and V_g, (19) can then be iteratively solved for I_{ds}. The theoretical curve obtained from (19) will be compared to experimental curves in Section IV.

In this model, the saturation current is defined as

$$\frac{I_{ds}}{qv_s n_s W} = 1. \quad (20)$$

Using a normalized parameter z,

$$z = \frac{I_{ds}}{qv_s n_s(V)W} \quad (21)$$

the saturation current can be calculated by

$$\int_{z_s}^{1} \frac{dz}{\partial\left[n_s(V)^{-1}\right]/\partial V \log[1-z]} = -\frac{E_s L_g I_{d\,\mathrm{sat}}}{qv_s W} \quad (22)$$

where $z_s = I_{d\,\mathrm{sat}}/qv_s W n_s(V_a)$. From (22) and (2), $I_{d\,\mathrm{sat}}$ can be calculated for different bias conditions. The saturation voltage can then be obtained by (2) and (20) as follows:

$$V_{d\,\mathrm{sat}} = V_g - V_{t0} - \frac{I_{d\,\mathrm{sat}}/qv_s W - C}{A + B\left[C - I_{d\,\mathrm{sat}}/qv_s W\right]} + I_{d\,\mathrm{sat}} R_d, \quad V_g - V_{d\,\mathrm{sat}} > V_p \quad (23a)$$

$$V_{d\,\mathrm{sat}} = V_g - V_{t0} - \frac{(d_i + d_d + \Delta d) I_{d\,\mathrm{sat}}}{\epsilon_{\mathrm{AlGaAs}} v_s W} + I_{d\,\mathrm{sat}} R_d, \quad V_g - V_{d\,\mathrm{sat}} \leqslant V_p. \quad (23b)$$

In the saturation region, the reduced channel length L_s can be determined by (15). The saturation region I–V characteristics can be calculated by replacing V_{ds} with $V_{d\,\mathrm{sat}}$, and L_g with $L_g - L_s$ in (19).

The expression for the most important parameter, the transconductance g_m, can be derived by the method proposed by Chang and Fetterman [18] as follows.

Condition 1:

$$g_m = \frac{I_{ds}\left[1 - f(z_s, z_d)\right]}{R_{\mathrm{eff}} I_{ds} + P(V_a) f(z_s, z_d) - P(V_c) + \log(1 - z_d)\left[\xi - \delta I_{ds}^2 \int_{z_s}^{z_d} Q(z)\, dz\right]} \quad (24a)$$

Condition 2:

$$g_m = \frac{I_{ds}\left[1 - f(z_s, z_d)\right]}{R_{\mathrm{eff}} I_{ds} + P(V_a) f(z_s, z_d) + V_b S(V_b) - V_c + \log(1 - z_d)\left[\xi - \delta I_{ds}^2 \int_{z_s}^{z_p} Q(z)\, dz\right]} \quad (24b)$$

Condition 3:

$$g_m = \frac{I_{ds}\left[1 - f(z_s, z_d)\right]}{R_{\mathrm{eff}} I_{ds} + V_a f(z_s, z_d) - V_c + \xi \log(1 - z_d)} \quad (24c)$$

where

$$\xi = E_s(L_g - L_s) \qquad \delta = 1/qv_s W$$

$$D = \epsilon_{\mathrm{AlGaAs}}/q(d_i + d_d + \Delta d)$$

$$z_p = \delta I_{ds}/DV_b \qquad z_d = I_{ds}/qv_s W n_s(V_c)$$

$$f(z_s, z_d) = \log(1 - z_d)/\log(1 - z_s)$$

$$f(z_p, z_d) = \log(1 - z_d)/\log(1 - z_p)$$

$$R_{\mathrm{eff}} = R_s\left[f(z_s, z_d) + R_d/R_s\right]$$

$$P(V) = (1 + BV)\left[(A + BC)V + C\right]/A$$

$$Q(z) = 2AB\delta/\left[z(A + BC) - \delta I_{ds} B\right]^2 \log(1 - z)$$

$$S(V_b) = f(z_p, z_d)\left[1 - D(1 + BV_b)^2/A\right].$$

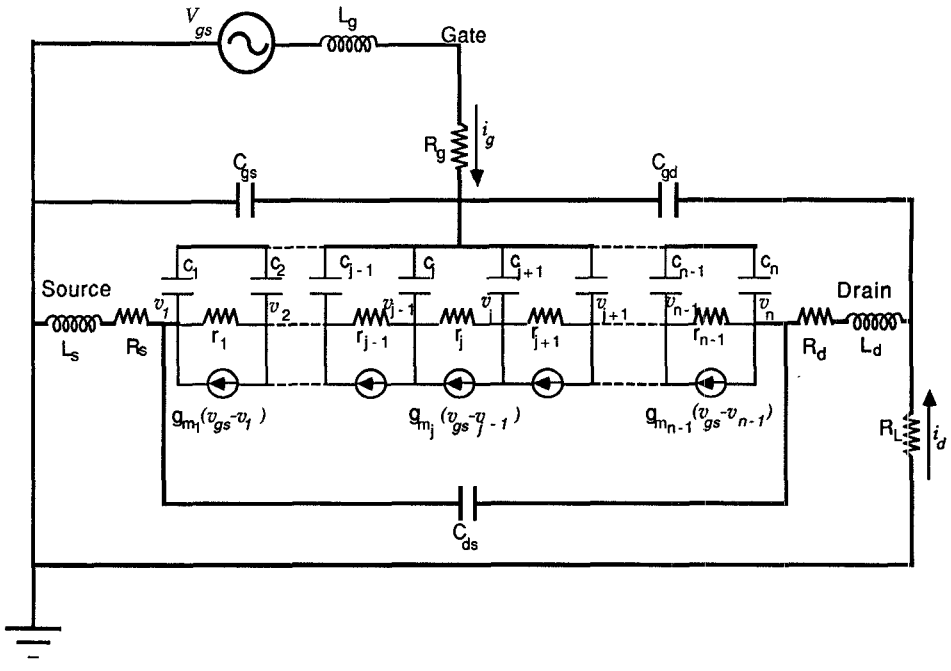

Fig. 4. Transmission line model for MODFET.

The simulated results of transconductance will be compared with Allied-Signal 0.3 μm HEMT's in Section IV.

Similar to the above model, another analytical nonlinear charge control model can be developed with less accuracy by employing (7) instead of (8). The result of that model will be presented [19] in the future.

III. Transmission Line Model for Microwave Frequency Analysis

The *RC* transmission lines are appropriate models for the investigation of frequency and transient response characteristics of certain microelectronic circuit components. Numerous examples exist for which the theory of *RC* lines has been applied to the study of thin-film and diffused resistors, capacitors, and conductors and to the evaluation of undesirable interactions between different components of integrated circuits. Moreover, *RC* lines can be successfully used to simulate the characteristics of certain active microcircuit elements, in particular, field-effect devices. To give some substance to this statement, note that a field-effect transistor may be considered to have two parts: 1) an active part associated with the 2DEG layer between the source and drain with transconductance g_m which is controlled by the gate voltage and 2) a passive part which includes nonlinear voltage-controlled resistances and capacitances.

The transmission line model we propose for high-frequency ac analysis is shown in Fig. 4. Since the good fit to dc experimental data gave us some confidence, the transmission line model is developed based on the analytical dc model. For each increment j in Fig. 4, the incremental capacitance c_j is modeled as

$$c_j = C_0 W dx \tag{25}$$

where $C_0 = \epsilon_{\mathrm{AlGaAs}}/(d_i + d_d + \Delta d)$, which is a constant by

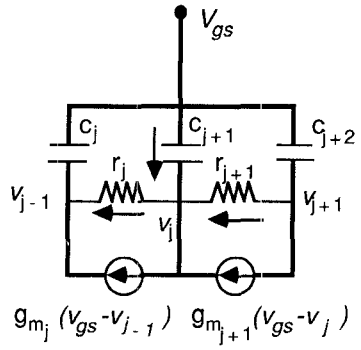

Fig. 5. Incremental cells of transmission line model.

assuming that the AlGaAs layer is completely depleted. This assumption is justified in the linear region of Fig. 2, where the maximum transconductance can be obtained. The incremental resistance r_j and the incremental transconductance g_{m_j} are modeled as follows:

$$r_j = \left[V_{j+1} - V_j\right]/I_{ds} \tag{26}$$

$$g_{m_j} = \beta V_{j+1}/\left[dx/L_g + \alpha V_{j+1}\right] \tag{27}$$

where V_j is the dc voltage along the channel. At each node of Fig. 4, Kirchhoff's current law is used for small-signal ac analysis, as shown in Fig. 5. For each node, the following equation is derived:

$$-\left(\frac{1}{r_j} + g_{m_j}\right)\tilde{v}_{j-1} + \left(\frac{1}{r_j} + \frac{1}{r_{j+1}} + j\omega_{c_{j+1}} + g_{m_{j+1}}\right)\tilde{v}_j - \frac{1}{r_{j+1}}\tilde{v}_{j+1} = \tilde{v}_{gs}\left(j\omega c_{j+1} + g_{m_{j+1}} - g_{m_j}\right) \tag{28}$$

where $\tilde{v}_j$ is the ac voltage. As shown in the above equation, the ac voltage at each node depends on the ac voltage

of the previous and the next node only. By applying Kirchhoff's current law to every node along the channel, the following tridiagonal linear equation can be obtained:

$$\begin{aligned} d_1\tilde{v}_1 + e_1\tilde{v}_2 &= b_1 \\ a_1\tilde{v}_1 + d_2\tilde{v}_2 + e_2\tilde{v}_3 &= b_2 \\ a_2\tilde{v}_2 + d_3\tilde{v}_3 + e_3\tilde{v}_4 &= b_3 \\ \ddots \quad \ddots & \quad \vdots \\ a_{N-1}\tilde{v}_{N-1} + d_N\tilde{v}_N &= b_N \end{aligned} \tag{29}$$

where

$$\begin{aligned} a_{j-1} &= -\left(1/r_j + g_{m_j}\right) \\ b_j &= \tilde{v}_{gs}\left[j\omega c_{j+1} + g_{m_{j+1}} - g_{m_j}\right] \qquad (j < N) \\ b_j &= \tilde{v}_{gs}\left[j\omega c_{j+1} - g_{m_j}\right] + \tilde{i}_d \qquad (j = N) \\ e_j &= -1/r_{j+1} \\ d_j &= 1/r_j + 1/r_{j+1} + j\omega c_{j+1} + g_{m_{j+1}}. \end{aligned}$$

The small-signal ac current and voltage distribution along the channel can be calculated by solving the above tridiagonal linear equation using the Gaussian elimination method. The terminal small-signal parameters are then determined by mixed parameters:

$$\tilde{i}_g = m_{11}\tilde{v}_{gs} + m_{12}\tilde{i}_d \tag{30}$$

$$\tilde{v}_{ds} = m_{21}\tilde{v}_{gs} + m_{22}\tilde{i}_d \tag{31}$$

where $\tilde{i}_g = \sum_{j=1}^{N}(\tilde{v}_{gs} - \tilde{v}_j)\,j\omega c_j$ and $\tilde{v}_{ds} = \tilde{v}_N$. By shorting the input circuit or opening the output circuit, the parameters m_{12} and m_{22} or m_{11} and m_{21} can be calculated respectively. The M parameters are then converted into S parameters. The calculated S parameters are compared with Allied-Signal 0.3 μm HEMT's in the next section.

This transmission line model can also be applied to GaAs MESFET's, the only difference being that in MESFET's the incremental capacitances should be voltage dependent.

IV. Comparison of Theory with the Measured Data

The low- and high-frequency characteristics of the standard depletion-mode devices are compared with the model results. It is demonstrated that the model parameters can be optimized to fit the $I-V$ characteristics and that the resulting parameters are reasonable. A comparison between measured ac S parameters is then made to determine the confidence level of our models.

A. Linear Charge Control Analytical dc Model

As stated earlier, the analytical model is valid only when the 2DEG is in the linear portion in Fig. 2, where maximum transconductance g_m can be obtained. The parameters used for comparing this model are listed in Table I, where L_g, W, d_l, d_d, μ_l, N_d, and R_s are the stated parameters of Drummond *et al.* [7]. They fabricated the

TABLE I

$L_g = 1.0\ \mu$m	$R_s = 12\ \Omega$
$W = 145\ \mu$m	$R_d = 30\ \Omega$
$d_l = 100$ Å	$R_p = 4$ kΩ
$d_d = 300$ Å	$E_0 = 3.0$ kV/cm
$\mu_l = 4300$ cm^2/V·s	$v_s = 1.2\times10^7$ cm/s
$N_d = 10^{18}$ cm^{-3}	$\phi_b = 1.106$ V

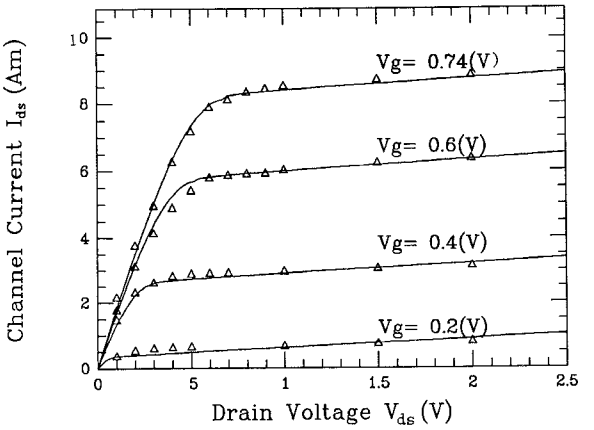

Fig 6. Comparison between the experimental and calculated $I-V$ characteristics. △: experimental data [7]; solid lines: calculations using analytical model developed.

HEMT using an $Al_{0.3}Ga_{0.7}As/GaAs$ heterostructure. As suggested by Chang [20], in order to include the current due to the parasitic resistance of the undoped GaAs buffer layer, the effective resistance $R_p = 4$ kΩ is chosen for the fit in the saturation region, and $R_d = 30\ \Omega$ is used. The threshold voltage is calculated as [18], [20]

$$V_{t0} = \phi_b - \frac{\Delta E_c}{q} + \frac{E_{f1}}{q} - \frac{qN_d d_d^2}{2\epsilon_{\mathrm{AlGaAs}}} \tag{32}$$

where $\epsilon_{\mathrm{AlGaAs}} = 12.2\epsilon_0$, $\Delta E_c = 0.32$ eV, and $\phi_b = 1.106$ V [18], [20]. In Fig. 6, the calculated output current–voltage characteristic using the analytical model is compared with the experimental data. The Δ symbols are the experimental data; the solid lines represent the calculated curves using the analytical model we developed. As one can see from this figure, the calculated results show excellent agreement with the experimental data in both the linear and the saturation region.

B. Nonlinear Charge Control dc Model

As a second example, our nonlinear charge control dc model is compared with the experimental data from [6]. The input parameters used for the comparison are listed in Table II, where L_g, W, d_l, d_d, n_{s0}, R_s, and R_d are the stated parameters of Yeager and Dutton. The parameters v_s, E_s, V_{t0}, p, and V_{ps} are optimized to fit the $I-V$ characteristics. $R_p = 4$ kΩ is also used to include the parasitic current in the AlGaAs layer. Fig. 7 shows a comparison between the calculated and measured data, where Δ is the experimental data, solid lines denote the calculated results of the our nonlinear charge control model, and the dashed lines represent the results calculated by Yeager and Dutton

TABLE II

$L_g = 1.0\ \mu m$	$V_{t0} = -0.42$ V
$W = 100\ \mu m$	$V_{ps} = 1.30$ V
$d_t = 30$ Å	$v_s = 2.25 \times 10^7$ cm/s
$d_d = 270$ Å	$E_s = 3.0$ kV/cm
$n_{s0} = 0.92 \times 10^{12}/cm^2$	$R_s = 8.4\ \Omega$
$p = 0.70$	$R_d = 8.4\ \Omega$

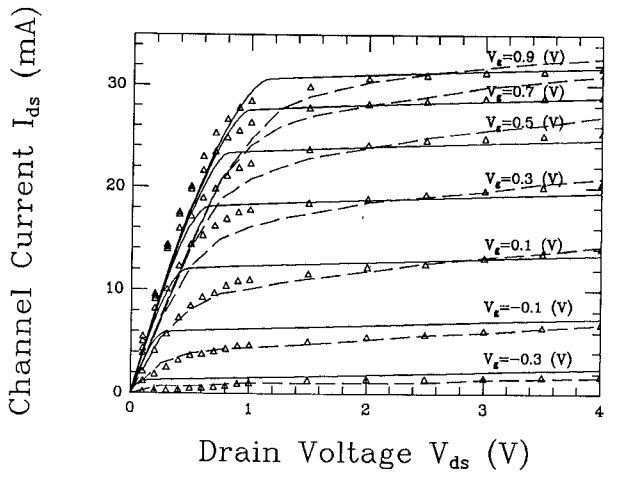

Fig. 7. Comparison between the experimental and calculated $I-V$ characteristics. △: experimental data [6]; solid lines: calculations using the nonlinear charge control model developed; dash lines: simulation results of [6].

[6]. In Fig. 7, we have some difficulty in obtaining a good fit with experimental data in the knee region. As can be seen from Fig. 7, the measured $I-V$ characteristics saturate earlier than the calculated data. The reason for this could be due to (8). As can be seen in Fig. 3, the curve for (8) is saturating later than the experimental data. In practical operation, to obtain the maximum transconductance, the device is always working in the saturation region. Hence the best fit in that region is conducted as shown in Fig. 7. Our models also agree with other experimental data, as shown in [21].

C. Nonlinear Charge Control Transconductance Model

A $0.3 \times 100\ \mu m^2$ gate HEMT fabricated on MBE-grown material from Allied-Signal is used as a sample to verify our transconductance model and the ac transmission line model in the next section. A 0.5 μm buffer layer was grown on a semi-insulating GaAs substrate followed by a 30 Å undoped space layer. Between this layer and the gate there is a 300-Å-thick AlGaAs layer with doping of $1.0 \sim 1.5 \times 10^{18}\ cm^{-3}$. Source-to-drain spacing is 1.25 μm. Since the exact nature of the traps and MBE doping transient were not fully characterized, the model parameters were optimized to match the transconductance characteristics. The results of the optimization are shown in Table III. The transfer characteristics (denoted by Δ) for a fixed drain voltage in the saturation region are shown in Fig. 8. The model calculation (solid line), using the material and device parameters already mentioned, is also shown in that figure. As can be seen from Fig. 8. the nonlinear charge control model closely fits the experimental results. The discrepancy for the positive gate voltage corresponding to maximum 2-D gas concentration could be attributed to hot electron effects that result in the transfer of energetic electrons from the 2-D channel to the AlGaAs or the buffer layer [22].

TABLE III

$L_g = 0.3\ \mu m$	$v_s = 1.13 \times 10^7$ cm/s
$W = 100\ \mu m$	$E_s = 2.0$ kV/cm
$d_t = 30$ Å	$p = 0.60$
$d_d = 300$ Å	$V_{t0} = -2.15$ V
$n_{s0} = 0.99 \times 10^{12}/cm^2$	$V_{ps} = 0.8$ V

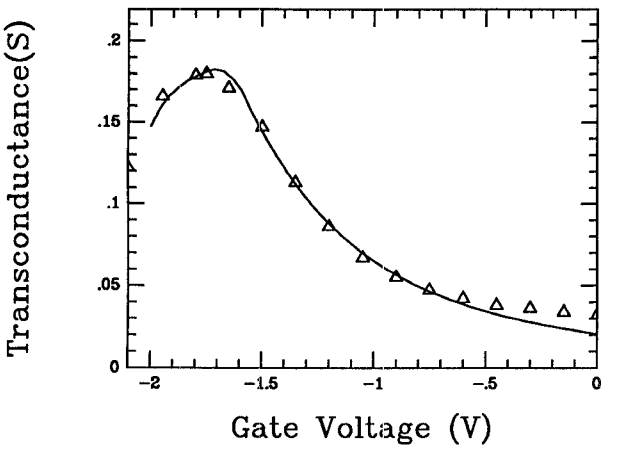

Fig. 8. The calculated and experimental transconductance of Allied Signal-Bendix 0.3 μm HEMT as a function of the gate voltage. △: experimental data at $V_d = 2.5$ V; solid lines: calculated curve.

TABLE IV

$L_g = 0.3\ \mu m$	$R_p = 0.8\ k\Omega$
$W = 100\ \mu m$	$V_{t0} = -2.20$ V
$d_t = 30$ Å	$V_g = -1.77$ V
$d_d = 300$ Å	$V_{ds} = 2.50$ V
$N_d = 1.3 \times 10^{18}\ cm^{-3}$	$C_{ds} = 0.02$ pF
$\mu_l = 4300\ cm^2/V \cdot s$	$C_{gd} = 0.01$ pF
$v_s = 1.6 \times 10^7$ cm/s	$C_{gs} = 0.02$ pF
$E_0 = 3.0$ kV/cm	$l_s = 0.01$ nH
$R_s = 8\ \Omega$	$l_g = 0.01$ nH
$R_d = 20\ \Omega$	$l_d = 0.01$ nH

D. Transmission Line Model for Microwave Frequency Analysis

Our aim is to reproduce the dc characteristics and microwave characteristics of a HEMT simultaneously. By fitting the dc characteristics, the optimum model parameters characterizing the device are obtained by using the analytical dc model developed in this paper. The same dc parameters are then used for the microwave model. The device parameters used for fitting the $I-V$ characteristics of the tested HEMT are listed in Table IV. Note that because the different models are used to fit the transfer

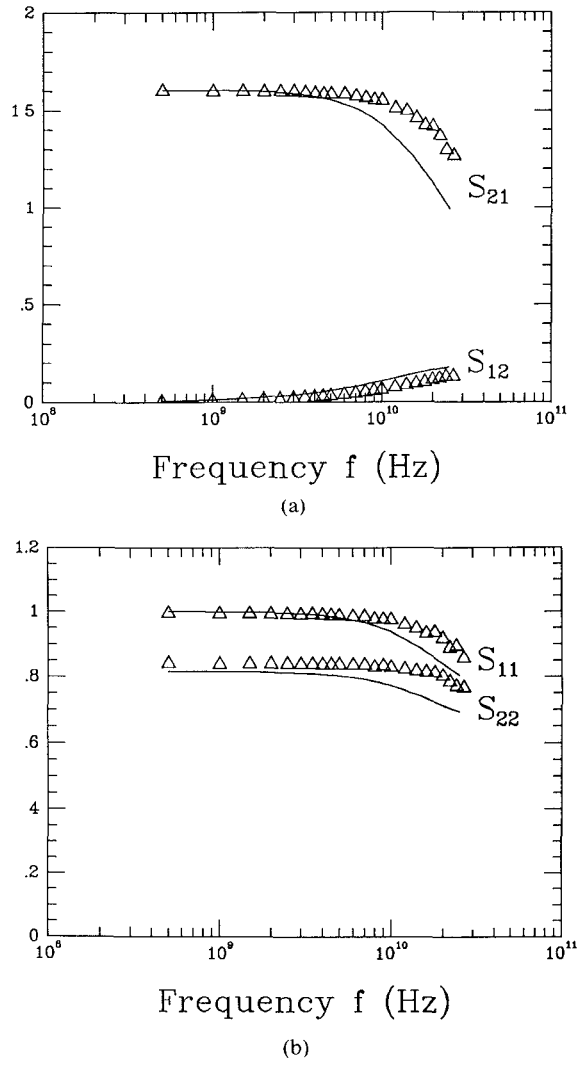

Fig. 9. The calculated and experimental S parameters (magnitude). Δ: experimental data; solid lines: calculations based on transmission line model. Device parameters are shown in Table IV.

characteristics and the $I-V$ characteristics for the same device (Allied-Signal 0.3×100 μm^3 HEMT), the fitting parameters are different in Tables III and IV. The extrinsic S parameters, including parasitics, are calculated for the bias condition of $V_g=-1.77$ V and $V_{ds}=2.5$ V, which is in the saturation region. The parasitic parameters are also listed in the Table IV. The S parameters are plotted as a function of frequency from 0.5 GHz up to 26 GHz in Fig. 9. The calculated curves (solid lines) fit the data (Δ) reasonably well. From Fig. 9(b), one can see that the measured S_{21} is larger than the calculated results at high frequencies. This increase of the transconductance can be attributed to an effective decrease of the source access resistance at microwave frequencies. The parasitic parameters R_s and R_d are obtained by optimizing the best fit of the $I-V$ characteristics. Then the optimized R_s is used as a constant in our ac transmission line model. The extrinsic transconductance $g_{m'}$ is related to the intrinsic transconductance g_m and the source resistance R_s by $g_{m'}=g_m/(1+g_mR_s)$. As recently reported by Roblin *et al.* [23], there is a notable decrease in the magnitude of R_s as the frequency varies from 1 to 30 GHz due to the fact that the contact resistivity is shunted by 2DEG depletion capacitance at high frequency. Such a frequency-dependent decrease in R_s can account for the increase of S_{21} at microwave frequencies.

E. Discussion

As the gate length become shorter, especially on the submicron scale, the gate length may no longer be considered much larger than the electron mean free path in the 2DEG channel. This is especially true at low temperature, where carrier dynamics are no longer dominated by polar optical phonon scattering and are almost free of impurity scattering. Non-steady-state transport may be included when one considers that the carrier drift velocity $v[E(x)]$ is not a local function of the electric field but rather of the local mean energy, and the local mean energy, a function of position as the distribution function of carriers in k-space, evolves gradually from the source to the drain under the gate [24]. In our one-dimensional dc models, this effect is not included. As a result, a much higher "effective" velocity (higher than the physical drift velocity) generally is needed in order to obtain a good fit with experimental data. It may be viewed as some "average velocity of the channel electron" and not a local velocity, especially on the submicron scale, when the geometry of the electric field is somewhat complicated. The limitations of these models arise from their one-dimensional characteristics and the fact that surface effects are neglected. The present models are based on a triangular well approximation but can easily be expanded to any other form of energy band discontinuity.

V. Conclusion

An analytical dc model is developed for the output $I-V$ characteristics with the more accurate velocity versus field empirical formula. The proposed analytical model for the HEMT's $I-V$ characteristics shows excellent agreement with experimental results. A simple empirical formula is introduced for nonlinear charge control of 2DEG, and hence a dc nonlinear charge control model is developed. The effects of both neutral donors in AlGaAs and channel electrons are included in the calculation though a unique nonlinear charge control model. A reasonable prediction of the transfer characteristics is achieved, which is very useful in predicting the maximum transconductance g_m.

We have also developed a model to calculate the S parameters for HEMT's. The analysis relies on the device parameters that are obtained by fitting the dc characteristics. The scattering parameters calculated are in reasonably good agreement with the experimental data. Further improvements were achieved by introducing parasitic capacitances and by optimizing the parasitic resistances and inductances at the source, drain, and gate.

In summary, a reasonable prediction of the microwave characteristics was achieved from the measured dc characteristics only. Our transmission line model is based on

physical parameters and therefore should be useful for estimating the microwave performance of HEMT's.

APPENDIX
DERIVATION OF EQUATION (11)

By substituting (1) to (10) in the text, one can derive

$$\frac{v(x)}{v_0} = \frac{I_{ds}}{\beta E_0 L_g \left[V_g - V_{t0} - V(x)\right]} \tag{A1}$$

where $\beta = \epsilon_{AlGaAs}\mu_l W/(d_i + d_d + \Delta d)L_g$.

By solving the electric field $E(x)$ in the quadratic equation (9), one can have

$$\frac{dV}{dx} = E(x) = E_0\left[\frac{v(x)}{v_0} - \frac{v_s}{v_0}\left(\frac{v(x)}{v_0}\right)^2\right]. \tag{A2}$$

In deriving the above equation, the approximation $\sqrt{1+x} \simeq 1 + x/2$ is used for $v(x)/v_0 < 1$. The third and higher orders of $v(x)/v_0$ are omitted.

Letting $t = 1/[V_g - V_{t0} - V(x)]$ in (A1) and substituting (A1) into (A2), one can get

$$\frac{dt}{t^3(1+bt)} = \frac{E_0 I_{ds}\, dx}{\beta V_c} \tag{A3}$$

where

$$b = I_{ds}R_0 v_s/v_0 = \left[V_g - V_{t0} - V(x)\right](v_s/v_0)(v(x)/v_0).$$

For high electron mobility transistors due to $v_0 = \mu_l E_0$, conditions $v_s/v_0 < 1$ and $v(x)/v_0 < 1$ hold in most cases. For the device biased in the linear portion of Fig. 2 before saturation, we have $V_g - V_{t0} - V(x) < 1$, so that the approximation $b < 1$ holds in general. Consider the following integration:

$$\int \frac{dt}{t^3(1+bt)} = \int \frac{dt}{t^3} - b\int \frac{dt}{t^2} + b^2 \int \frac{dt}{t(1+bt)}. \tag{A4}$$

For $b^2 \ll 1$, the last term of the above equation can be omitted. Integrating (A3) from source to drain using (A4), one can obtain

$$\frac{I_{ds}E_0 L_g}{\beta V_c} = -\frac{1}{2t^2}\Big|_{t_1}^{t_2} + \frac{b}{t}\Big|_{t_1}^{t_2} \tag{A5}$$

where $t_1 = 1/(V_g - V_{t0} - V_s)$, $t_2 = 1(V_g - V_{t0} - V_d)$, and $V_s = I_{ds}R_s$. After manipulation, one can derive (11) in the text.

REFERENCES

[1] N. J. Shak, S. S. Pei, C. W. Tu, and R. C. Tiberio, "Gate length dependence of SSI circuits using submicrometer selectively doped heterostructure transistor technology," *IEEE Trans. Electron Devices*, vol. ED-33, pp. 543–547, 1986.

[2] T. Henderson *et al.*, "Microwave performance of a quarter micrometer gate low noise pseudomorphic InGaAs/AlGaAs MODFET," *IEEE Electron Devices Lett.*, vol. EDL-7, p. 649, 1986.

[3] P. Saunier and J. W. Lee, "High efficiency millimeter wave GaAs/AlGaAs power HEMT's," *IEEE Electron Devices Lett.*, vol. EDL-7, p. 503, 1986.

[4] N. T. Linh, "Two-dimensional electron gas FET's: Microwave applications," in *Semiconductors & Semimetals*, R. K. Willardson and A. C. Beer, Eds., vol. 24. New York: Academic Press, 1985.

[5] P. Roblin, S. Kang, A. Ketterson, and H. Morkoc, "Analysis of MODFET microwave characteristics," *IEEE Trans. Electron Devices*, vol. ED-34, pp. 1919–1928, 1987.

[6] H. R. Yeager and R. W. Dutton, "Circuit simulation model for the high electron mobility transistor," *IEEE Trans. Electron Devices*, vol. ED-33, pp. 682–692, 1986.

[7] T. J. Drummond, H. Morkoc, K. Lee, and M. Shur, "Model for modulation doped field effect transistor," *IEEE Electron Devices Lett.*, vol. EDL-3, pp. 338–341, 1982.

[8] H. Rohdin and P. Roblin, "A MODFET dc model with improved pinchoff and saturation characteristics," *IEEE Trans. Electron Devices*, vol. ED-33, pp. 664–672, 1986.

[9] M. Weiss and D. Pavlidis, "The influence of device physical parameters on HEMT large-signal characteristics," *IEEE Trans. Microwave Theory Tech.*, vol. 36, pp. 239–249, 1988.

[10] W. A. Hughes and C. M. Snowden, "Nonlinear charge control in AlGaAs/GaAs modulation doped FET's," *IEEE Trans. Electron Devices*, vol. ED-34, pp. 1617–1625, 1987.

[11] F. N. Trofimenkoff, "Field-dependent mobility analysis of the field effect transistor," *Proc. IEEE*, vol. 53, pp. 1765–1766, 1965.

[12] R. A. Giblin, E. F. Scherer, and R. L. Wierich, "Computer simulation of instability and noise in high-power avalanche devices," *IEEE Trans. Electron Devices*, vol. ED-20, pp. 404–418, 1973.

[13] H. Kroemer, "The Gunn effect under imperfect cathode boundary conditions," *IEEE Trans. Electron Devices*, vol. ED-15, pp. 819–837, 1968.

[14] J. G. Ruch and G. S. Kino, "Measurement of the velocity-field characteristics of gallium arsenide," *Appl. Phys. Lett.*, vol. 10, pp. 40–42, 1967.

[15] B. Carnez, A. Cappy, A. Kaszinski, E. Constant, and G. Salmer, "Modeling of submicron gate field-effect transistor including effects of non-stationary electron dynamics," *J. Appl. Phys.*, vol. 51, pp. 784–790, 1980.

[16] S. Tiwari, "Performance of heterostructure FET's in LSI," *IEEE Trans. Electron Devices*, vol. ED-33, pp. 554–563, 1986.

[17] K. Park and K. D. Kwack, "A model for the current-voltage characteristics of MODFET's," *IEEE Trans. Electron Devices*, vol. ED-33, pp. 673–676, 1986.

[18] C. S. Chang and H. R. Fetterman, "Analytical model for high-electron mobility transistor," *Solid-State Electron.*, vol. 30, pp. 485–491, 1987.

[19] D. H. Huang and H. C. Lin, "Analytical model for MODFET with 2DEG nonlinear charge control," submitted for publication.

[20] C. S. Chang and H. R. Fetterman, "Analytical model for HEMT's using new velocity–field dependence," *IEEE Trans. Electron Devices*, vol. ED-34, pp. 1456–1462, 1987.

[21] D. H. Huang, "Modeling GaAs field effect transistor's," Ph.D. dissertation, University of Maryland, 1989.

[22] A. Eskandarian, "Determination of the small-signal parameters of a AlGaAs/GaAs MODFET," *IEEE Trans. Electron Devices*, vol. 35, pp. 1793–1801, 1988.

[23] P. Roblin, L. Rice, S. B. Bibyk, and H. Morkoc, "Nonlinear parasitics in MODFET's and MODFET I–V characteristics," *IEEE Trans. Electron Devices*, vol. 35, pp. 1207–1801, 1988.

[24] G. Salmer, J. Zimmermann, and R. Fauqembergue, "Modeling of MODFET's," *IEEE Trans. Microwave Theory Tech.*, vol. 36, pp. 1124–1140, 1988.

Di-Hui Huang (S'88) was born in Beijing, China. He received the B.S. and the M.S. degrees in semiconductor physics from Xian Jiaotong University, Xian, China, in 1982 and 1984, respectively. He is currently working towards the Ph.D. degree in electrical engineering at University of Maryland, College Park. His research interests are in the area of semiconductor devices for integrated circuit application. His current work focuses on device modeling, especially in GaAs MESFET's and MODFET's.

Hung Chang Lin (S'47–A'52–M'56–SM'65–F'69–LF'85) received the B.S. degree in electrical engineering from Chiaotung University in China in 1941, the M.S.E. degree from Michigan in 1948; and the doctor of electrical engineering degree from the Polytechnic Institute of Brooklyn in 1956.

From 1941 to 1946, he worked in China as an engineer at the Central Radio Works and Central Broadcasting Administration. From 1948 to 1956, he engaged mostly in transistor work as a research engineer at RCA Laboratories. In 1956 he joined the Hytron Division of Columbia Broadcasting System, where he worked until 1959 as Manager of the Semiconductor Applications Laboratory. From 1959 to 1969, he was with the Westinghouse Electric Corporation working on integrated circuits, in various capacities as Advisory Engineer at the Research Development Laboratory, Manager of Advanced Development at the Molecular Electronics Division, and Consultant to the System Development Division.

Dr. Lin is the holder of 46 U.S. patents, the author of the book *Integrated Electronics* and some 120 technical articles, and coauthor of two other books. He served as Associate Editor of the IEEE JOURNAL OF SOLID-STATE CIRCUITS and has been a Technical Program Committee member and/or session chairman in numerous International Solid State Circuits conferences and International Electron Device meetings. He is also a member of the Sigma Xi Honor Society and Phi Tau Phi Honor Society. He was the recipient of the 1978 J. J. Ebers Award of the IEEE Electron Devices Society. In the academic field, he was a part-time Adjunct Professor at the University of Pittsburgh and a Visiting Lecturer at the University of California at Berkeley. Presently, he is a Professor at the University of Maryland.

He was elected a Fellow of the Institute of Electrical and Electronics Engineers "for contributions to semiconductor electronics and circuits and pioneering of integrated circuits."